D_{3d} Ground-State Structure of $V(CO)_6$: A Combined Matrix Isolation and ab Initio Study of the Jahn−Teller Effect

Eduard Bernhardt,*,† Helge Willner,*,† Andreas Kornath,§ Jürgen Breidung,‡ Michael Bühl,‡ Volker Jonas,‡ and Walter Thiel*,‡

Gerhard-Mercator-Universität Duisburg, Fakultät 4, Anorganische Chemie, Lotharstrasse 1, D-47048 Duisburg, Germany, Max-Planck-Institut für Kohlenforschung, Kaiser-Wilhelm-Platz 1, D-45470 Mülheim/ Ruhr, Germany, and Universität Dortmund, Institut für Anorganische Chemie, Otto-Hahn-Strasse 6, D-44227 Dortmund, Germany

Received: August 7, 2002; In Final Form: November 13, 2002

Structures, relative energies, vibrational spectra, and ESR parameters of the 17e$^-$ molecule $V(CO)_6$ in O_h, D_{3d}, D_{4h}, and D_{2h} symmetry have been computed with density functional and high-level ab initio methods. At all theoretical levels applied, the same energetic order is obtained, $D_{3d} < D_{2h} < D_{4h} < O_h$, with the D_{2h} structure as a transition state connecting equivalent D_{3d} species. At the RCCSD(T)/AE2 level using UBP86/AE2 geometries, the energies of the D_{2h}, D_{4h} and O_h species relative to that of D_{3d} minimum are predicted to be 210, 535, and 731 cm^{-1}, respectively. According to molecular dynamics simulations on the UBP86/AE1 potential energy surface, the D_{3d} minimum is preserved at very low temperatures (around 16 K), whereas at 300 K the molecule is highly fluxional with an averaged structure indistinguishable from that of $[V(CO)_6]^-$ with its O_h symmetric ground state. Nearly complete IR and Raman spectra of $V(CO)_6$ and $V(^{13}CO)_6$ have been recorded at 300 K for the first time in the gas phase, in solution, and at cryogenic temperatures in Ne and Ar matrices. The spectra show a pronounced temperature dependence, especially for the Jahn−Teller active modes, E_g and T_{2g}. The observed infrared matrix spectra generally agree well with the calculated spectrum (BP86/AE2 level) for the D_{3d} structure and much less with that of the D_{4h} isomer. The A_{1g} modes in the Raman spectra are reasonably well reproduced computationally in the harmonic approximation, whereas this approximation breaks down for the E_g and T_{2g} bands, as expected. Further evidence for the D_{3d} symmetry of $V(CO)_6$ is obtained from a reanalysis of the experimental ESR spectrum that is reported in the literature. The observed ordering of the hyperfine coupling constants $A_{\parallel}$ and $A_{\perp}$ is reproduced theoretically only when distortion to D_{3d} symmetry is assumed. In addition, the bonding properties of $V(CO)_6$ are compared to those of $[V(CO)_6]^-$ and $Cr(CO)_6$.

1. Introduction

The first synthesis of vanadium hexacarbonyl dates back to 1959.[1,2] It is the only homoleptic transition-metal carbonyl that exists near room temperature as a free radical; therefore, its molecular and spectroscopic properties have been investigated intensively. Magnetic susceptibility measurements of solid $V(CO)_6$ have shown that this molecule has one unpaired electron and that for temperatures lower than 66 K a weak antiferromagnetic coupling ($J = -50$ cm^{-1}) exists.[3] As the $^2T_{2g}$ ground state of a d^5 system is three-fold degenerate, a distorted octahedral geometry should be present, in accordance with the Jahn−Teller theorem.[4−6] To clarify this question and to characterize its molecular properties, $V(CO)_6$ has been studied in different aggregation states with different techniques: IR[7−11] UV−vis[7,12,13], ESR,[14−18] MCD,[12] and PE[19] spectroscopy as well as electron[20] and X-ray diffraction.[21] These investigations show that $V(CO)_6$ is subject to a dynamical Jahn−Teller effect and has nearly octahedral geometry at room temperature. The amount of static distortion, which should appear at lower temperatures, has been discussed controversially. For the electron diffraction data, the vibrational amplitudes, which are larger than for $Cr(CO)_6$, are in accordance with a dynamic distortion to D_{4h} or D_{3d} symmetry.[20] The X-ray data at −30 °C indicate a small tetragonal distortion ($V-C_{ax} = 1.993(2)$ Å, $V-C_{eq} = 2.005(2)$ Å) that may also be due to crystal packing effects. The ESR results also do not provide a consistent picture.[14−18] According to the most recent work,[18] $V(CO)_6$ exists in a CO matrix at 4 K in axial symmetry (D_{4h} or D_{3d}).

All published infrared work has been limited to the infrared-active CO band (ν_6): the splitting of the octahedral T_{1u} band has been interpreted in favor of a D_{4h} distortion,[7−11] without regarding matrix splitting or a possible D_{3d} distortion. The FTIR spectrum of this band at higher resolution (0.01 cm^{-1}) for supersonic jet-cooled $V(CO)_6$ molecules does not show resolved rovibrational lines but only three broad subbands.[22] On the theoretical side, orbital energies of $V(CO)_6$ have been obtained from SCF-Xα-DV calculations,[13] and CO substitution reactions have been simulated by SCF-Xα-DV[23] and CISD//HF[24] calculations. More recently, the geometry and the harmonic vibrational frequencies of $V(CO)_6$ (D_{3d}) have been computed[25] by density functional theory (B3LYP) in the context of modeling electron-transfer rates in $[Co(Cp)_2][V(CO)_6]$.[25−27]

This paper reports an extensive theoretical and experimental study of the Jahn−Teller distortion in $V(CO)_6$. We first describe the computational methods that have been applied (section 2)

* To whom correspondence should be addressed. E-mail: e.bernhardt@uni-duisburg.de. willner@uni-duisburg.de. thiel@mpi-muelheim.mpg.de.
† Gerhard-Mercator-Universität Duisburg.
§ Universität Dortmund.
‡ Max-Planck-Institut für Kohlenforschung.

10.1021/jp021835u CCC: $25.00
Published on Web 01/17/2003

SCHEME 1: Sketch of Possible Distortions from O_h Symmetry in $V(CO)_6$

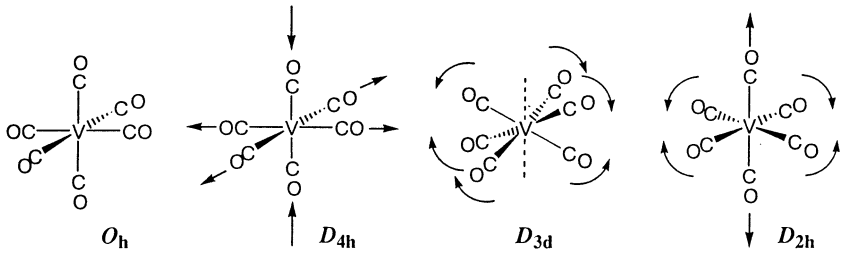

and then present the calculated structures, energies, vibrational spectra, and ESR parameters as well as the results from Born−Oppenheimer molecular dynamics simulations (section 3). After specifying the experimental methods used (section 4), we present and assign the observed matrix infrared and Raman spectra (section 5). Finally, we discuss the available theoretical and spectroscopic evidence that supports a D_{3d} ground state of $V(CO)_6$ (section 6).

2. Theoretical Methods

Gradient-corrected unrestricted density functional calculations[28] were carried out by using the Gaussian 94[29] and Gaussian 98[30] program systems. Gradient corrections for exchange and for correlation were taken from the work of Becke[31] and Perdew,[32] respectively (usually abbreviated as BP or BP86). Two basis sets were employed, labeled AE1 and AE2. Both use a (14s11p6d)/[8s7p4d] all-electron basis set from Wachters[33] for the 3d transition metal augmented with two additional 4p functions[33] and a diffuse d function.[34] For carbon and oxygen, AE1 employs the 6-31G(d) basis,[35−37] whereas AE2 uses a (10s,6p)/[5s,3p] triple-ζ basis for C and O[38] supplemented by two sets of d polarization functions.[39] Spherical d functions were applied throughout. Geometries were optimized at the UBP86/AE1 and UBP86/AE2 levels within the chosen point-group symmetry (O_h, D_{3d}, D_{4h}, D_{2h}). The resulting structures were characterized by analytical second derivative calculations[30] that yield the harmonic vibrational frequencies and the infrared and Raman intensities. This computational approach is analogous to the restricted BP86 calculations in our previous studies on transition-metal carbonyls.[40,41]

Open-shell coupled cluster calculations [42−44] were carried out with MOLPRO[45] using restricted open-shell Hartree−Fock reference functions.[44] Geometries were optimized with single and double substitutions and the AE1 basis (RCCSD/AE1). Single-point energy evaluations at BP86 and RCCSD optimized structures included a perturbational estimate of the effects of connected triple excitations[46] and employed both basis sets (RCCSD(T)/AE1 and RCCSD(T)/AE2).

Born−Oppenheimer molecular dynamics (MD) simulations were performed for neutral $V(CO)_6$ and anionic $[V(CO)_6]^-$ at the unrestricted and restricted RI-BP86/AE1 levels, respectively, making use of the resolution-of-identity (RI) approximation as implemented in the TURBOMOLE program,[47] together with suitable auxiliary basis sets,[48,49] and a medium-sized grid (grid 3).[50] Starting from an optimized structure, MD simulations were performed with TURBOMOLE[47] using the ChemShell interface[51] for microcanonical ensembles with a time step of 1 fs. The simulations were run for 2.5 ps at an average temperature of ca. 300 K and for 4.5 ps at ca. 16 K (average temperatures in the NVE runs after initial, instantaneous heatup). In each case, data sampling was started after the first 0.5 ps, which were taken for equilibration.

Hyperfine coupling constants (HFCCs) and g tensors were computed using BP86/AE1 geometries, BP86 and B3LYP[52,53] density functionals, and AE1 and U1 basis sets, the latter denoting a fully decontracted version of the former. In the final SCF iteration, grid 4 was used,[50] except for BP86/U1, which employed grid 5 throughout.[50] These ESR computations were performed with the ORCA program package.[54]

3. Theoretical Results

3.1. Static Calculations. According to group theory, the linear Jahn−Teller effect of octahedral ground-state $V(CO)_6$ involves T_{2g} and E_g modes.[4−6] It will lower the symmetry from O_h ($^2T_{2g}$ state) either to D_{3d} ($^2A_{1g}$ state) or to D_{4h} ($^2B_{2g}$ state), and the transition structures between the D_{3d} minima will have D_{2h} symmetry ($^2B_{3g}$ state). Consequently, we have considered structures with O_h, D_{3d}, D_{4h}, and D_{2h} symmetry (Scheme 1). All calculations refer to the electronic ground state that was determined either without constraints (Gaussian 98) or by imposing the appropriate electronic state symmetry in the largest Abelian subgroup (MOLPRO: D_{2h} for O_h and D_{4h}, C_{2h} for D_{3d}).

Table 1 lists the calculated optimized geometries of $V(CO)_6$ as well as the available experimental data from electron diffraction[20] and X-ray analysis.[21] For the sake of comparison, it also includes theoretical and experimental structures for two related octahedral species—the closed-shell $[V(CO)_6]^-$ anion and the isoelectronic $Cr(CO)_6$ molecule.

It is obvious that the applied computational approaches yield qualitatively similar structures in each case. The tetragonal distortion of $V(CO)_6$ from O_h to D_{4h} always leads to a compressed structure with a shorter VC bond in the axial position. The trigonal distortion to D_{3d} changes the CVC angle only slightly from the octahedral reference angle of 90° (by about 4°) while keeping the VCO moiety almost linear (to about 1°). The same applies for the D_{2h} structure where the deviation of the CVC angle from 90° is slightly larger (about 5−6°). The UBP86/AE1 and UBP86/AE2 bond lengths are similar (with similar trends as found previously [40,41,57]) and thus exhibit no pronounced basis set sensitivity. A comparison of the UBP86/AE1 and RCCSD/AE1 bond lengths shows that the latter are somewhat shorter for CO (by about 0.013 Å) and significantly longer for VC (by 0.03−0.05 Å). This suggests that larger basis sets are needed to converge the RCCSD calculations (which, however, is not affordable at present). However, there is excellent agreement between the UBP86/AE1 and RCCSD/AE1 bond angles, which are thus expected to be reliable.

Experimentally, the vapor-phase electron diffraction data for $V(CO)_6$ have been interpreted in terms of a regular octahedral structure and a dynamic Jahn−Teller effect.[20] The X-ray data indicate a "marginally significant tetragonal distortion" for the VC and CO bond lengths (uncorrected for librational motion), but this distortion may also be due to crystal packing effects.[21] The experimental VC bond lengths[20,21] are in the same range as those calculated at the UBP86 level whereas the RCCSD values are systematically somewhat larger (see Table 1). In an overall assessment, the UBP86/AE2 structures would thus seem to be most realistic.

TABLE 1: Experimental and Calculated Bond Lengths (Å) and Angles (deg) for $V(CO)_6$, $[V(CO)_6]^-$, and $Cr(CO)_6$[a]

molecule	method	M−C^1	M−C$^2_{(ax)}$	C^1−O^1	C^2−O$^2_{(ax)}$	C^1−M−C$^{1'}$	M−C^1−O^1
$V(CO)_6$							
	exptl X-ray[b]	2.005(2)	1.993(2)	1.123(2)	1.136(3)		
	exptl ED[c]	2.015(2)		1.138(2)			
O_h	UBP86/AE1	2.0017		1.1641			
	UBP86/AE2	2.0042		1.1537			
	RCCSD/AE1	2.0434		1.1508			
D_{4h}	UBP86/AE1	2.0169	1.9739	1.1622	1.1676		
	UBP86/AE2	2.0201	1.9750	1.1516	1.1577		
	RCCSD/AE1	2.0652	2.0033	1.1485	1.1554		
D_{3d}	UBP86/AE1	2.0011		1.1641		94.2	179.2
	UBP86/AE2	2.0038		1.1537		94.7	178.7
	RCCSD/AE1	2.0435		1.1507		93.9	179.3
	B3LYP[d]	2.0187		1.1410		93.7	179.4
D_{2h}	UBP86/AE1	1.9929	2.0188	1.1652	1.1617	95.2	179.1
	UBP86/AE2	1.9952	2.0223	1.1550	1.1510	95.8	178.7
	RCCSD/AE1	2.0328	2.0662	1.1519	1.1483	95.3	179.1
$[V(CO)_6]^-$							
O_h	expt[e]	1.945(7)		1.148(7)			
	BP86/AE1	1.9632		1.1796			
	BP86/AE2	1.9637		1.1701			
$Cr(CO)_6$							
O_h	expt[f]	1.918(2)[e]		1.141(2)			
	BP86/AE1	1.9122		1.1639			
	BP86/AE2	1.9113		1.1537			

[a] For D_{4h} and D_{2h}, C^1−O^1 is in the equatorial position, and C^2−O^2 is in the axial position. For D_{3d}, C^1−M−C$^{1'}$ represents the angle between two COs connected by the C_3 symmetry axis. For D_{2h}, C^1−M−C$^{1'}$ represents the angle between two pairs of equatorial COs. Only those angles that are different from 90 or 180° are given. [b] Reference 21. [c] Reference 20. [d] References 25 and 26. [e] Reference 55. [f] Reference 56.

TABLE 2: Calculated Relative Energies (cm^{-1}) for $V(CO)_6$

geometry[a]	energy[b]	D_{3d}	D_{2h}[c]	D_{4h}	O_h[d]
UBP86/AE1	UBP86/AE1	0	318	818	965
	RCCSD(T)/AE1	0	126	350	539
UBP86/AE2	UBP86/AE2	0	332	839	1000
	RCCSD(T)/AE1	0	112	332	525
	RCCSD(T)/AE2	0	210	535	731
RCCSD/AE1	RCCSD/AE1	0	108	273	525
	RCCSD(T)/AE1	0	136	371	560

[a] Method used for geometry optimization (see Table 1). [b] Method used for energy evaluation; zero-point vibrational corrections are not included. [c] Transition structure with one imaginary frequency. [d] Not a stationary point.

In the case of $[V(CO)_6]^-$ and $Cr(CO)_6$, there is also good agreement between the observed and calculated BP86 structures. In these 18-electron complexes, the metal−C bond length is significantly shorter than in the 17-electron $V(CO)_6$ radical. This may be attributed to the fact that there is one electron less to provide π back-donation in $V(CO)_6$, which should lead to a weaker and longer VC bond. However, an analogous effect is not seen for the CO bond (Table 1).

Table 2 presents the calculated relative energies for the different structures of $V(CO)_6$. All chosen approaches yield qualitatively the same energetic order: $D_{3d} < D_{2h} < D_{4h} < O_h$. Force constant analysis at the UBP86 level confirms that the D_{3d} and D_{4h} species are minima on the potential surface whereas the D_{2h} structure is a transition state connecting equivalent D_{3d} species (see below). The relative energies from UBP86/AE1 and UBP86/AE2 are quite similar whereas those from RCCSD/AE1 are more closely spaced. Our most reliable estimates of relative energies are expected to come from single-point RCCSD(T)/AE2 calculations (which are still feasible): using the preferred UBP86/AE2 geometries, the energies of the D_{2h}, D_{4h}, and O_h species relative to the D_{3d} minimum are predicted to be 210, 535, and 731 cm^{-1}, respectively. The corresponding UBP86/AE2 values are 332, 839, and 1000 cm^{-1}, respectively, whereas a recent B3LYP study [25] puts the D_{2h} species at 207 cm^{-1}.

The calculated vibrational wavenumbers, infrared and Raman intensities, and ^{13}CO isotopic shifts for the D_{3d} and D_{4h} minima of $V(CO)_6$ are given in the Supporting Information (Tables S1 and S2, respectively) both at the UBP86/AE1 and UBP86/AE2 levels. Since these results are based on the harmonic approximation, they should be unreliable for the Jahn−Teller active modes (E_g, T_{2g}). For other modes, especially for the infrared-active vibrations of ungerade symmetry, they are expected to be as realistic as previously found for related molecules.[40,41,57] The theoretical results for the vibrational spectra will be discussed in more detail during the assignment of the experimental spectra (section 6).

The harmonic force constants of transition-metal carbonyls provide a sensitive probe for π-back-donation effects.[58] Table S3 of the Supporting Information presents selected internal force constants of $V(CO)_6$, $[V(CO)_6]^-$, and $Cr(CO)_6$ that indeed confirm (see above) that the π back-donation is smaller in the 17-electron $V(CO)_6$ radical than in the 18-electron species $[V(CO)_6]^-$ and $Cr(CO)_6$. This can be seen, for example, from the small values of F_{MC} and F_{MCO} (see ref 58 for a more detailed discussion).

3.2. Molecular Dynamics Simulations. To study the effect of thermal averaging on the geometrical parameters, we performed MD simulations on the Born−Oppenheimer surface. An unconstrained geometry optimization for $V(CO)_6$ was first conducted at the RI-BP86 level. Starting from an octahedral arrangement, a minimum with effective D_{3d} symmetry was obtained, consistent with the energetic ordering of the stationary points at the DFT levels. In the subsequent MD simulations starting from this minimum, the system was first heated to very low, cryogenic temperatures, around 16(±6) K. At this temperature, the system essentially stayed within the potential well of the initial D_{3d} minimum. Two distinct sets of C−V−C angles, which fluctuated around 94(±4) and 86(±4)°, were discernible. This result is consistent with a static Jahn−Teller (JT) distortion, at least on the 4-ps time scale of the simulation.

When the MD simulation was repeated at room temperature, around 300(±70) K, much larger amplitudes for the bending modes were found. After 2 ps, the average values of all of the C−V−C angles fell in the range between 88 and 92°, with maximum deviations around ±20°. Since the values for the 12

TABLE 3: Computed ESR Parameters[a] of $V(CO)_6$

symmetry	level of theory	$A_{\|\|}$	$A_\perp$	A_{iso}	$g_{\|\|}$	$g_\perp$	g_{iso}
D_{4h}	BP86/AE1	−181.4	−63.4	−102.8	1.998	2.242	2.161
	B3LYP/AE1	−187.9	−64.1	−105.4	1.995	2.209	2.137
	B3LYP/U1	−178.2	−55.6	−96.5			
D_{3d}	BP86/AE1	−1.4	−124.2	−83.3	2.001	2.048	2.033
	B3LYP/AE1	+0.3	−129.3	−86.1	2.001	2.056	2.038
	B3LYP/U1	+7.8	−121.2	−78.2			
expt[b]		21(3)	143.8(6)		1.98(2)	2.111(1)	

[a] Hyperfine couplings (HFCCs) A (MHz) and g tensors. [b] From ref 18; no absolute signs were derived for the HFCCs and g's.

C−V−C bond angles were rather evenly spaced at any time, no structures corresponding to particular, well-defined symmetries could be observed along the trajectory.

For comparison, the same MD simulations were performed for $[V(CO)_6]^-$. Because JT effects are absent, this anion possesses a single O_h-symmetric minimum. At ca. 300 K, the molecule appeared to be as flexible as neutral $V(CO)_6$, as judged from the amplitudes of the C−V−C bending ($90 \pm 20°$).

The degree of flexibility of both neutral and anionic species is reflected in the computed radial distributions displayed in Figure 1. At 16 K (top of Figure 1), well-resolved peaks are obtained, marking the bonded and nonbonded separations in relatively rigid molecules. On going from the O_h-symmetric anion (dashed line) to the D_{3d}-symmetric neutral species (solid line), the splitting of some of the nonbonded separations due to symmetry lowering is clearly visible. At 300 K, in contrast, both radial distributions are virtually indistinguishable (middle of Figure 1). For instance, the peaks between 2.5 and 3 Å, which correspond to the $C\cdots C_{cis}$ distances, have blended into a single broad band. Both radial distributions are in good qualitative accord with that of gaseous $V(CO)_6$, obtained by electron diffraction[20] at a slightly higher temperature (bottom of Figure 1).

We are aware of the limitations of this MD-based approach, as a rigorous treatment of electronic−vibrational couplings in JT systems may need to go beyond the Born−Oppenheimer (or adiabatic) approximation and a classical treatment of the nuclei.[4−6] However, salient experimental observables in JT systems have been reproduced computationally on the basis of related MD simulations (for instance, $Cu^{2+}(aq)$[59] and $C_2H_6^+$-(g)[60]). Possible limitations notwithstanding, our MD results support the qualitative interpretation that a static JT distortion in $V(CO)_6$ can be observed only at very low temperatures. At room temperature, dynamical averaging is so rapid that the resulting mean structure is indistinguishable from that of the corresponding anion with its O_h-symmetric equilibrium geometry.

3.3. Electron Spin-Resonance Parameters. In a recent ESR study of $V(CO)_6$ isolated in a CO matrix at 4 K, g values and hyperfine parameters were interpreted in terms of an axially distorted octahedral molecule.[18] Apparently, only a D_{4h} distortion was considered. To determine if the D_{3d} minimum could also be reconciled with the experimental data, we have computed the ESR parameters of the two minima at appropriate DFT levels (Table 3). The theoretical g tensors (last three columns in Table 3) are not conclusive: with the B3LYP functional, which performs best for most transition-metal compounds studied so far,[61,62] $g_\perp$ (and thus g_{iso}) is considerably over- and underestimated for the D_{4h} and D_{3d} forms, respectively,[63] with maximum errors of 98 and 55 ppt, respectively. Even though such errors are significantly larger than usually found for transition-metal complexes, similar deviations can occur in exceptional cases.[61,62]

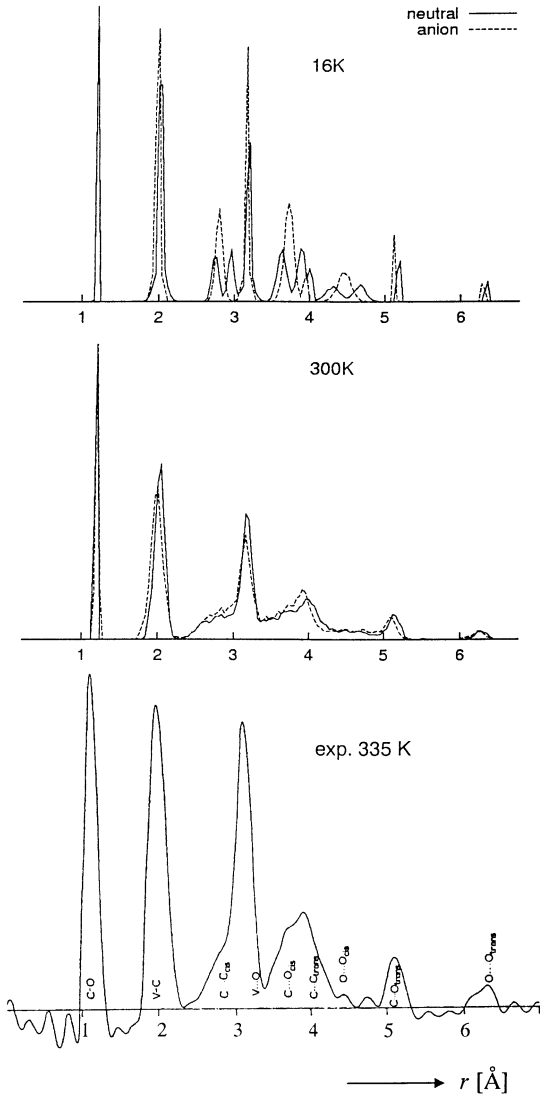

Figure 1. Radial distributions obtained from MD simulations at ca. 16 K (top) and at ca. 300 K (middle); bottom: experimental radial distribution from ref 20 (reprinted with permission from Elsevier Science, copyright 1975). (—) $V(CO)_6$; (- -) $[V(CO)_6]^-$.

Thus, no definite structural assignment can be made on the basis of the theoretical g tensors.

The HFCCs, in contrast, are more significant. Whereas for the D_{4h} form $A_{\|}$ is predicted to be much larger in absolute terms than $A_\perp$, the opposite is found for the D_{3d} minimum. Only the latter ordering is in accord with experiment (Table 3). Since theoretical HFCCs can strongly depend on the flexibility of the basis set employed, we also performed computations with a large uncontracted basis (U1 in Table 3), which afforded no qualitative change.[64] Note that the absolute signs of $A_{\|}$ and $A_\perp$ have not

been determined experimentally but that opposite signs have been taken for these two.[18] Assuming a negative sign for the largest component, as suggested by the computations, the largest error for the D_{3d} structure is around 23 MHz or 16% for $A_\perp$ (B3LYP/U1), similar to what is presently achievable for transition metals (see, for instance, ref 65). The D_{4h} form gives much larger quantitative deviations (on the order of 200 MHz when the different signs of $A_{||}$ and $A_\perp$ are taken into account) and does not reproduce the experimental HFCC tensor even qualitatively. Thus, the computed HFCCs strongly support the assignment of the species in the ESR experiment to the D_{3d} form, in accord with the energetic ordering.

4. Experimental Section

4.1. Instrumentation. The matrix infrared spectra were recorded on a Bruker IFS 66v FTIR instrument in reflectance mode using a transfer optic. A DTGS detector and a KBr/Ge beam splitter were used in the 5000−400-cm^{-1} region. Scans (64) were added for each spectrum using apodized resolutions of 1.2 or 0.3 cm^{-1}. A far-IR DTGS detector and a 6-μm Mylar beam splitter were used in the 440−80-cm^{-1} region. Scans (128 or 64) were added for each spectrum using apodized resolutions of 1.2 or 0.3 cm^{-1}, respectively. Details of the matrix apparatus have been described elsewhere.[66]

The gas-phase infrared spectra were recorded with the same instrument using a resolution of 2 cm^{-1} in the 5000−400 cm^{-1} range. The storage vessel containing the $V(CO)_6$ sample was directly connected to the evacuated IR gas cell (optical pass length 200 mm; Si windows 0.5 mm thick) contained in the sample compartment of the evacuated FTIR instrument. By varying the temperature, different amounts of $V(CO)_6$ were introduced into the cell just for the period of measurement and were immediately removed afterward by evacuation.

For matrix measurements, small amounts of pure $V(CO)_6$ samples (ca. 0.1 mmol) were transferred in vacuo into a small U-trap kept at −30 °C. This U-trap was mounted in front of the matrix support and was allowed to reach a temperature in the range of −35 to −45 °C. A gas stream (1 to 4 mmol h^{-1}) of argon or neon was directed over the solid $V(CO)_6$, and the resulting gas mixture was immediately quenched on the matrix support at 12 and 5 K, respectively. Altogether, 20 matrices of different amounts (1 to 5 mmol) and concentrations were prepared and investigated. The photolysis experiments were carried out by using a high-pressure mercury lamp (TQ 150, Heraeus) in combination with a water-cooled quartz lens optic and a $\lambda > 280$-nm cut-off filter (Schott).

For reference purposes, matrices containing $Cr(CO)_6$ were prepared in a similar way, but in this case, the U-trap was kept at −42 °C.

After the matrix experiments, the remaining $V(CO)_6$ was dissolved in benzene under an argon atmosphere. A Raman spectrum of the resulting yellow-green solution was recorded in the 4000−100-cm^{-1} range using a spectral resolution of 4 cm^{-1} on a Bruker FRA 106 Raman spectrometer and the 1064-nm excitation line of a Nd:YAG laser (100 mW).

Details of the matrix apparatus for recording Raman spectra have been described elsewhere.[67] Altogether, eight argon matrices were prepared in the same manner as described above, yielding matrices of a 100-μm thickness and estimated sample-to-argon ratios of 1:1000. The spectra were recorded using a resolution of 1.2 cm^{-1} and the 514.5-nm excitation line of an Ar^+ ion laser operating at 500 mW. Annealing of the matrices for 5 min at 40 K led to an improvement of the S/N ratio and caused no changes in the line profiles.

4.2. Synthesis of $V(CO)_6$. $V(CO)_6$ was obtained by a method described in the literature from $[Na(diglyme)_2][V(CO)_6]$ (Strem Chemicals) and phosphorus acid.[68] A glass reactor ($V \approx 30$ mL) fitted with a 10-mm valve with a PTFE stem (POR-10, Young, London) was cooled to −20 °C and loaded with 5 g of H_3PO_4 (~90%) and 100 mg of $[Na(diglyme)_2][V(CO)_6]$. The reactor was connected to an evacuated U-trap held at −40 °C. Upon warming to room temperature, the reaction proceeded with hydrogen evolution under dynamic vacuum, and solid black $V(CO)_6$ covered the inner surface of the U-trap. The crude product was transferred into another small U-trap held at −30°C in vacuo, forming small black shiny crystals. At room temperature, $V(CO)_6$ decomposes within hours but can be stored for months at −20 °C.

The synthesis of $V(^{13}CO)_6$ was performed starting from $[n\text{-}Bu_4N][V(^{13}CO)_6]$.[69] A 200-mL glass bulb fitted with a 10-mm valve with a PTFE stem (POR-10, Young, London) was loaded under an argon atmosphere with a magnetic stirring bar with 10 mL of tetrahydrofuran, 100 mg of vanadium trichloride (Fluka), and 100 mg of sodium. After cooling the content to −196 °C, the bulb was evacuated, and 100 mg of cyclooctatetraene (Fluka) and 3 mmol of ^{13}CO (>99%, IC Chemicals) were introduced in vacuo. The reaction proceeded at 40 °C over 20 h with stirring. The yellow suspension was filtered in a syringe, and the resulting clear solution was added dropwise to a solution of 300 mg of $[n\text{-}Bu_4N][HSO_4]$ (Merck) and 100 mg of NaOH in 30 mL of water. Subsequently, the precipitated $[n\text{-}Bu_4N][V(^{13}CO)_6]$ was filtered off, dried in vacuo, and washed with 1 mL of ether. The product (200 mg, 70% yield) was transferred into a 20-mL reactor and treated with excess HCl (g) at −80 °C. Black $V(^{13}CO)_6$ was formed and sublimed under dynamic vacuum into a small U-trap held at −30 °C.

Commercially available $Cr(CO)_6$ (Fluka) was used for the matrix experiments after sublimation in vacuo.

5. Experimental Results

Infrared and Raman spectra of $V(CO)_6$ have been recorded both at room temperature and isolated in a Ne matrix at 5 K and in an Ar matrix at 12 K. Typical spectra are presented in Figure 2 and are compared to the matrix spectra of $Cr(CO)_6$, which are in good agreement with literature spectra.[70,71] All spectra have been reproduced several times with different samples, and in addition, spectra for $V(^{13}CO)_6$ have been recorded under the same conditions to clarify the vibrational assignments further. A comparison of the $V(CO)_6$ spectra, obtained in Ne and Ar matrices, reveals that the fine structure of several bands is due to matrix splittings, which are generally smaller in a Ne than in an Ar matrix. The relative band intensities and bandwidths are very similar in both matrices.

Tables 4 and 5 list the vibrational wavenumbers, intensites, and ^{13}CO shifts as observed in the matrix infrared and Raman spectra, respectively, and the corresponding theoretical predictions for the D_{3d} and D_{4h} minima are included for comparison.

Photolysis experiments clearly show that the bands between 4000 and 400 cm^{-1} belong to $V(CO)_6$ because the photolysis of matrix-isolated samples with light of $\lambda > 280$ nm results in a uniform decrease of all IR bands assigned to $V(CO)_6$. At the same time, the yellow Ne matrix becomes dark brown, and new absorptions appear at 2144 cm^{-1} (free CO) and 1964, 1957, 1870, and 2098 cm^{-1}, which can be assigned by comparison with literature spectra to $V(CO)_5$ (1963, 1959 cm^{-1}),[76] $[V(CO)_6]^-$ (1873 cm^{-1}),[76] and $[V(CO)_6]^+$ (2070 cm^{-1}).[11] The dark-brown color is presumably caused by the charge-transfer complex

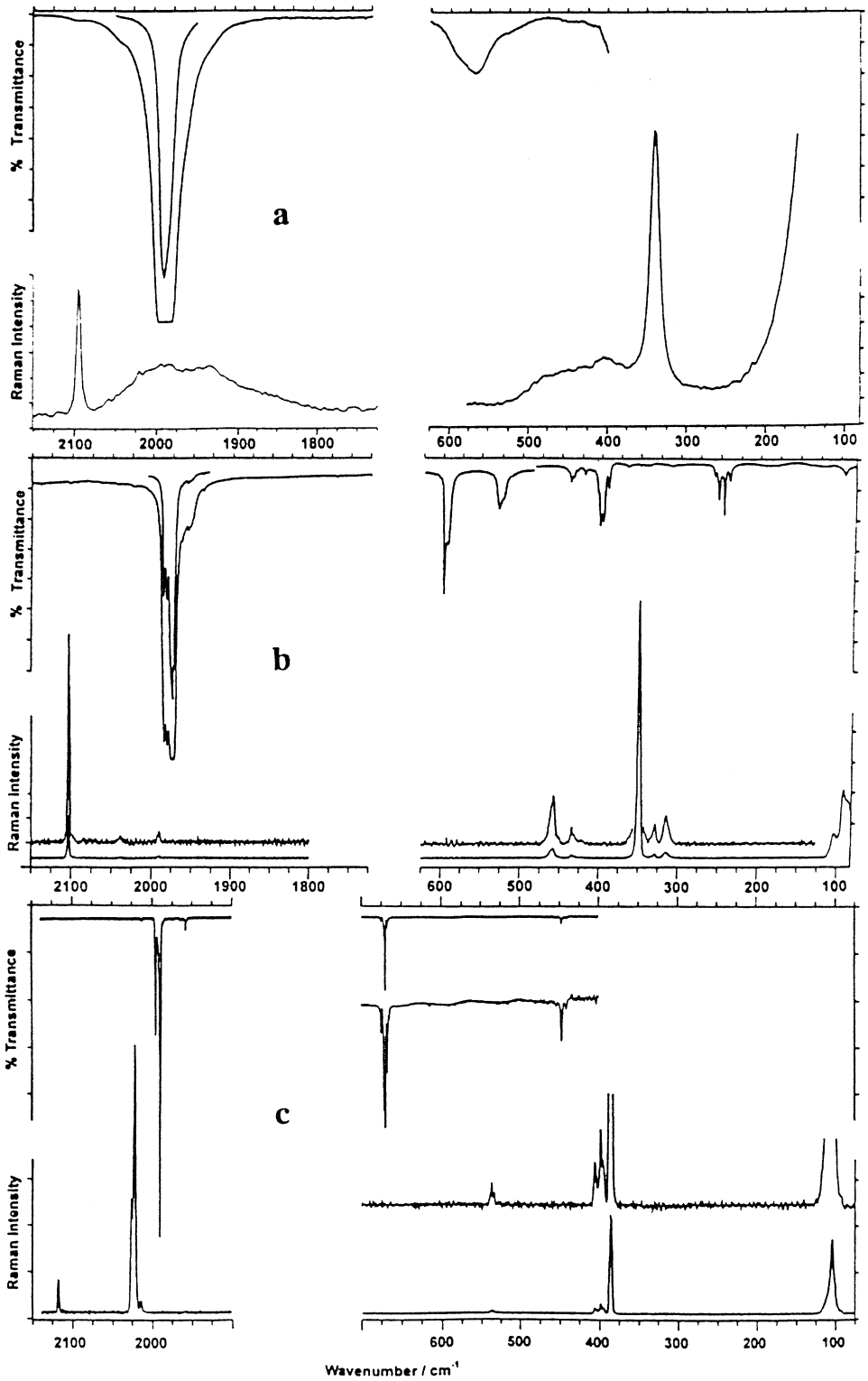

Figure 2. Vibrational spectra of $V(CO)_6$ and $Cr(CO)_6$. (a) IR gas-phase spectrum of $V(CO)_6$ and Raman spectrum of $V(CO)_6$ diluted in benzene at room temperature. (b) IR and Raman spectrum of $V(CO)_6$ isolated in an Ar matrix at 12 K. (c) IR and Raman spectrum of $Cr(CO)_6$ isolated in an Ar matrix at 12 K

$[V(CO)_6]^+[V(CO)_6]^-$, which has also been suggested to be the reason for the dark color of solid $V(CO)_6$ itself.[13]

Although the two molecules $V(CO)_6$ and $Cr(CO)_6$ differ only by one electron, the Jahn−Teller effect causes the spectra to be very different. Moreover, the spectra for $V(CO)_6$ show an amazing temperature dependence (Figure 2a and b). The single ν(CO) band in the IR gas-phase spectrum at room temperature is split in an Ar matrix into two components (with additional matrix site splittings), as observed by others.[9,11] The broad IR band in the gas phase around 580 cm^{-1} seems to consist of three components whereas in the Ar or Ne matrix there are only two components exhibiting additional small matrix site splittings. Even more pronounced are the differences in the Raman spectra. The very broad and strong signals at 2050−1850 cm^{-1} and 500−350 cm^{-1} in benzene solution (Figure 2a), recorded at room temperature, drop in intensity extremely in the Ar matrix (Figure 2b). There are only two weak signals at 2038.0 and 1988.9 cm^{-1} at matrix temperatures in the spectrum of the ^{12}C

TABLE 4: IR Spectra of $V(CO)_6$

assignment	D_{3d}, theory					expt, Ar-matrix,12 K				expt, Ne-matrix, 5 K				D_{4h}, theory				
O_h		ν, cm^{-1}	I^a	$\Delta\nu^b$	$\Delta^{13}C$	ν, cm^{-1}	I^c	$\Delta\nu^b$	$\Delta^{13}C$	ν, cm^{-1}	I^c	$\Delta\nu^b$	$\Delta^{13}C$		ν, cm^{-1}	I^a	$\Delta\nu^b$	$\Delta^{13}C$
ν_{CO}, T_{1u}	ν_8, A_{2u}	1972	1374	2	44.6	1983.9	52	7.7	43.8	1990.7	54	6.1	44.0	A_{2u}	1951	1859	−31	44.2
	ν_{17}, E_u	1970	3595		44.4	1976.2	100		43.7	1984.6	100		43.5	E_u	1982	3138		44.6
δ_{VCO}, T_{1u}	ν_{18}, E_u	621	230	82	12.6	598.0	8.4	68.8	12.6	596.6	11.3	67.6	12.2	E_u	595	181	−42	13.5
	ν_9, A_{2u}	539	83		9.1	529.2	3.5		10.5	529.0	3.0		10.1	A_{2u}	637	128		12.2
δ_{VCO}, T_{2u}	ν_5, A_{1u}	502	0	50	17.2	n.o.				n.o.				B_{2u}	474	0	101	15.8
	ν_{19}, E_u	452	4		12.2	439.3	0.7		12.5	437.5	0.6		12.2	E_u	373	2		10.7
ν_{VC}, T_{1u}	ν_{20}, E_u	409	30	6	10.3	397.9	5.9	0	9.4	396.0	2.7	0	8.0	E_u	438	34	−4	9.3
	ν_{10}, A_{2u}	403	3.4		8.8	(397.9)				(396.0)				A_{2u}	442	12		8.8
δ_{CVC}, T_{1u}	ν_{21}, E_u	85	2.7	12	0.4	95	0.5		0	95	0.5		0	E_u	84	2	5	0.4
	ν_{11}, A_{2u}	73	0.7		0.3	n.o.				n.o.	-			A_{2u}	79	0.7		0.3
δ_{CVC}, T_{2u}	ν_6, A_{1u}	63	0	17	0.3	n.o.				n.o.				B_{2u}	40	0	−5	0.3
	ν_{22}, E_u	46	0.9		0.3	n.o.				n.o.				E_u	45	0		0.2

[a] km mol^{-1}. [b] Splitting of the T modes. [c] Relative integrated intensity.

TABLE 5: Raman Spectra of $V(CO)_6$ Isolated in an Ar Matrix, 12 K

assignment	D_{3d}, theory					expt				D_{4h}, theory				
O_h		ν, cm^{-1}	I^a	$\Delta\nu^b$	$\Delta^{13}C$	ν, cm^{-1}	I^c	$\Delta\nu^b$	$\Delta^{13}C$		ν, cm^{-1}	I^a	$\Delta\nu^b$	$\Delta^{13}C$
ν_{CO}, A_{1g}	ν_1, A_{1g}	2072	132		48.4	2102.0	12.5		47.2	A_{1g}	2074	92		48.4
ν_{CO}, E_g	ν_{12}, E_g	1960	832	0	44.5	2038.0 ?	0.8	49		B_{1g}	2009	261	37	46.3
						1988.9 ?	1.8			A_{1g}	1972	268		45.6
δ_{VCO}, T_{2g}	ν_{13}, E_g	471	2.6	20	16.5	457.5?[d]	10.4	24.3	11.2	E_g	713	0.0	405	26.9
	ν_2, A_{1g}	451	1.1		15.8	433.2?[d]	2.6		3.9	B_{2g}	408	0.2		14.2
ν_{VC}, A_{1g}	ν_3, A_{1g}	358	55		5.8	348.8	100		5.3	A_{1g}	349	36		5.8
ν_{VC}, E_g	ν_{14}, E_g	344	11	0	6.1	312.2?[d]	4.9		4.0	A_{1g}	381	27	28	6.2
										B_{1g}	353	13		5.9
δ_{VCO}, T_{1g}	ν_7, A_{2g}	345	0	18	10.3	n.o.				A_{2g}	302	0	−41	9.1
	ν_{15}, E_g	327	0.5		9.6	328.0	2.1		7.3	E_g	343	0.0		10.4
δ_{CVC}, T_{2g}	ν_{16}, E_g	76	23	1	0.3	102.2?	sh	16.7	0.4	E_g	109	17	39	0.2
	ν_4, A_{1g}	75	10		0.3	90.3?	99.6		−0.2	B_{2g}	70	9		0.3
						85.5 ?	sh		0.5					

[a] $Å^4$ amu^{-1}. [b] Splitting of T and E modes. [c] Relative integrated intensity. [d] The vibrations are probably coupled with the electronically excited D_{3d} state (spin−orbit coupling) and are therefore not pure vibrations. Consequently, the isotopic shift is too low. The band at 433.2 cm^{-1} may be a nearly pure electronic transition.

species and no band at all in the spectrum of the ^{13}C species. The Raman signal around 400 cm^{-1} splits in an Ar matrix into four components. The relative intensity of the IR band at 250 cm^{-1} depends on the matrix material, and its position is shifted on isotopic substitution. Therefore, an impurity seems to be unlikely for this band. The same holds true for the weak infrared band of $V(^{13}CO)_6$ at 360 cm^{-1}.

It is interesting that a similar temperature dependence in the Raman spectra has been observed for the E modes of OsF_6, which also exhibits a dynamic Jahn−Teller distortion.[72−75]

We now discuss the assignment of the fundamental bands by making use of the theoretical predictions for the vibrational spectra.

6. Discussion

To interpret the observed spectra, we first discuss the possible Jahn−Teller distortions of $V(CO)_6$. In the linear approximation,[4−6] the Jahn−Teller effect of the T_{2g} ground state involves E_g and T_{2g} modes, which result in D_{4h} and D_{3d} distortions, respectively. Compared with the O_h structure, the energies of the three D_{4h} and four D_{3d} minima are lower by $E_{JT}(E)$ and $E_{JT}(T)$, respectively. The distortion will be tetragonal in the case of $E_{JT}(E) > E_{JT}(T)$ and trigonal otherwise. The transition state between two minima has D_{2h} symmetry and lies below the O_h structure by $[E_{JT}(E) + 3E_{JT}(T)]/4$. In the quadratic approximation,[4−6] the topology may remain the same, or the six D_{2h} transition structures may become minima.

TABLE 6: Calculated Jahn−Teller Energies (cm^{-1}) for $V(CO)_6$

energy[a]	geometry[b]	$E_{JT}(T)$	$E_{JT}(E)$	$\Delta E(D_{2h})$[c]
UBP86/AE2	UBP86/AE2	1000	161	122
UBP86/AE1	UBP86/AE1	965	147	114
RCCSD(T)/AE2	UBP86/AE2	731	196	76
RCCSD(T)/AE1	RCCSD/AE1	560	189	44
RCCSD(T)/AE1	UBP86/AE1	539	189	38
RCCSD/AE1	RCCSD/AE1	525	252	40
RCCSD(T)/AE1	UBP86/AE2	525	192	29

[a] Method used for energy evaluation; zero-point vibrational corrections are not included. [b] Method used for geometry optimization (see Table 1). [c] $\Delta E(D_{2h}) = E(D_{2h}) - (E(D_{4h}) + 3E(D_{3d}))/4$.

Taking spin−orbit coupling into account, the $^2T_{2g}$ term of octahedral $V(CO)_6$ is split into $E_{2g}' + G_g'$, with E_{2g}' being the ground state. In the linear approximation,[4−6] the molecule will remain octahedral (O_h) as long as the Jahn−Teller energies $E_{JT}(E)$ and $E_{JT}(T)$ remain sufficiently small relative to the spin−orbit coupling constant ξ: $E_{JT} < 0.667\xi$ leads to O_h symmetry only; $E_{JT} = 0.667\xi$ to 0.75ξ results in O_h and D_{3d} or D_{4h}; and $E_{JT} > 0.75\xi$ leads to D_{3d} or D_{4h} symmetry only.

The theoretical relative energies of the different $V(CO)_6$ structures (Table 2) are easily converted to Jahn−Teller energies E_{JT} (Table 6). In the case of $V(CO)_6$, with an experimental spin−

TABLE 7: ESR Data at 4 K for $V(CO)_6$ and Related Complexes

parameter	$V(CO)_6$, CO matrix		$V(N_2)_6$, N_2 matrix		$Nb(CO)_6$, CO matrix		$Nb(N_2)_6$, N_2 matrix	
point group	D_{3d}		D_{4h}		D_{3d}		D_{4h}	
$g_\perp$[a]	−2.111(1)		−2.032(1)		−2.2212(5)		−2.0958(9)	
$g_\parallel$[a]	1.98(2)		1.965(1)		1.959(1)		1.9505(5)	
$A_\perp$,[a] MHz	143.8(6)		153(3)		193(1)		238(2)	
$A_\parallel$,[a] MHz	21(3) [−21][c]		−332(1)		−111(3)		−448(1)	
ω [b]	0	0.004	0	0.0046	0	−0.004	0	0.0056
E_{JT}/ξ[d]	3.77	3.98	2.68	20.08	2.90	2.80	2.40	6.42
k[d]	0.64	0.76	0.18	0.90	0.97	0.88	0.39	0.91
K_k,[d] MHz	−107 [−117][c]	−107 [−117][c]	−223	−215	−189	−190	−333	−320
B,[d] MHz	68 [50][c]	67 [50][c]	70	57	41	42	78	65

[a] $|g|$ and $|A|$ from ref 18; note that the signs correspond to the convention adopted in ref 79, which differs from that of refs 54 and 61 used to generate the data in Table 3. [b] For a definition of the parameter ω, see ref 79; results for two limiting, estimated values are shown. [c] There is an alternative sign for $A_\parallel$ possible, resulting in alternative values given in brackets. [d] Calculated values.

orbit coupling constant of about 100 cm^{-1},[78] the computed Jahn−Teller energies yield $E_{JT}(T)/\xi > 5$ and $E_{JT}(E)/\xi > 1$, implying that Jahn−Teller distortions will occur. However, $Ta(CO)_6$ is not expected to distort since E_{JT} and ξ are around 500 cm^{-1} and 2000 cm^{-1}, respectively, which leads to an E_{JT}/ξ ratio of about 0.25.

We next attempt to determine from the observed infrared and Raman spectra (Tables 4 and 5) whether $V(CO)_6$ actually distorts to a D_{3d} or D_{4h} minimum. For this purpose, we assign the spectra with the help of the theoretical predictions (Tables S1 and S2) by making use of the computed frequencies, intensities, and ^{13}CO isotopic shifts. The latter are usually calculated quite reliably for related systems[40,41] and are very sensitive to the type of vibration involved.

The observed infrared spectra of $V(CO)_6$ generally agree as well as expected[40,41,57] with the calculated spectrum of the D_{3d} structure and much less so with that of the D_{4h} structure. In the CO stretching region, the less intense A_{2u} band is observed ca. 6−8 cm^{-1} above the more intense degenerate band (E_u), consistent with the theoretical D_{3d} results (analogous split of 2 cm^{-1}) and in contrast to the theoretical D_{4h} results (opposite ordering with a split of −31 cm^{-1}); the deviations between experiment and theory are in the usual range[40,41,57] for D_{3d} but not for D_{4h}. Even more striking are the comparisons for the two infrared bands in the region between 530 and 600 cm^{-1} where the position of the less intense A_{2u} band (ν_9, 529 cm^{-1}) is reproduced to within 10 cm^{-1} for D_{3d} and is missed by more than 100 cm^{-1} for D_{4h}; moreover, the measured ^{13}CO isotopic shifts match those for D_{3d} much better. In the range between 450 and 500 cm^{-1}, the weak band seen at 439.3 cm^{-1} can be assigned to the ν_{19} mode of the D_{3d} structure (E_u, predicted at 452 cm^{-1}), which is also supported by the ^{13}CO isotopic shifts whereas there is no fully satisfactory assignment for this band in D_{4h}. Around 400 cm^{-1}, a single infrared band is observed, which according to the calculations should primarily be attributed to the ν_{20} mode of the D_{3d} structure (E_u, 409 cm^{-1}) since the close-lying ν_{10} mode (A_{2u}, 403 cm^{-1}) is predicted to be much weaker. Again, the observed data are not as well matched by the calculated frequencies for D_{4h}. Finally, in the region below 100 cm^{-1}, only one band is observed at 95 cm^{-1}, which corresponds to ν_{21}.

In an overall judgment, the assignment of the observed infrared spectra is consistent only with the theoretical predictions for the D_{3d} minimum. The agreement between theory and experiment is about as good as in previous studies of closed-shell transition-metal carbonyls.[40,41,57] This may seem surprising at first sight since the Jahn−Teller distortions in $V(CO)_6$ should complicate the situation significantly. However, all infrared-active modes are of ungerade symmetry whereas the Jahn−Teller modes are of gerade symmetry. As a consequence, the infrared-active modes can apparently still be described satisfactorily within the usual harmonic approximation, which must break down for the Jahn−Teller active modes E_g and T_{2g}.

Hence, for the Raman spectrum, the agreement between calculated and observed spectra cannot be as good as for the infrared spectra. The calculated numerical results are documented in Table 5. Those for the A_{1g} modes still seem reasonable, while those for the Jahn−Teller active modes (E_g and T_{2g}) are partly nonsensical, as expected (see, e.g., the intensities for ν_{12}). Under these circumstances, we prefer to avoid a more detailed comparison for the Raman spectra and rely on the infrared spectra for identifying the D_{3d} ground state of $V(CO)_6$.

The relative energies of the D_{3d} and D_{4h} structures will be influenced by zero-point vibrational energy corrections that have not been considered so far (Table 2). Given the failure of the harmonic approximation for the Jahn−Teller active modes (see above), we have determined these corrections from the computed harmonic wavenumbers of the other modes only (i.e., including all modes from Table 4 and the A_{1g} and T_{1g} modes from Table 5). This leads to a relative stabilization of the D_{4h} structure by 40 cm^{-1}; therefore, our best estimate for its energy relative to the D_{3d} minimum decreases from 535 cm^{-1} (Table 2, RCCSD(T)/AE2) to 495 cm^{-1}.

Many ESR studies on $V(CO)_6$ have been performed in strongly interacting matrix materials such as $Cr(CO)_6$ or cyclohexane.[15−17] In such cases, the lattice distortion on the isolated $V(CO)_6$ molecule may be greater than the Jahn−Teller distortion, leading to nonaxial ESR spectra. However, for $V(CO)_6$ isolated in a CO matrix at 4 K, further evidence for D_{3d} symmetry can be obtained from a deeper analysis of the experimental ESR spectrum.[18] Our analysis is based on a minimum-basis-set ligand-field model of g tensors and hyperfine couplings in octahedral low-spin d^5 complexes.[79] Within the framework of this model, both experimental ESR parameters, the g tensors $g_\perp = g_x = g_y$ and $g_\parallel = g_z$, and the hyperfine coupling constants $A_\perp = A_x = A_y$ and $A_\parallel = A_z$ can be used to estimate (i) the energies Δ (splitting of the d_π level in an axial ligand field) and Δ_{te} (difference between d_π and d_σ levels in an approximately octahedral d^5 complex), (ii) the spin−orbit coupling constants ξ and ξ_{te} inside d_π and between the d_π and d_σ levels, (iii) the k-orbital reduction factor, and (iv) the Fermi contact term K_k and the parameter for dipole−dipole interaction $P = P_d$ (for d electrons).

The combination of the parameters ξ_{te} and Δ_{te} gives the new parameter $\omega = \xi_{te}/\Delta_{te}$, which is a measure of the mixing between the d_π and d_σ levels by spin−orbit coupling. With increasing σ bonding, the ω values strongly decrease. The parameters K_k

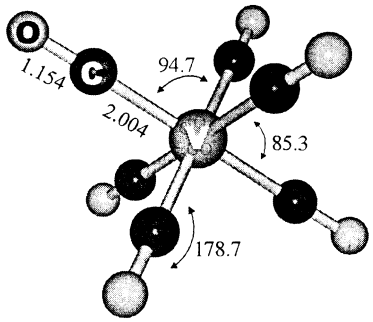

Figure 3. D_{3d} equilibrium structure of $V(CO)_6$ including salient parameters optimized at the UBP86/AE2 level (distances in Angstroms, angles in degrees). The view is perpendicular to the three-fold axis, and the upper and lower "tripods" are equivalent by symmetry.

and P are related to the Hamiltonian $H_{HFS} = K_k(S^*J) + P\{3(S^*r_0)(J^*r_0) - (S^*J) + k_1(L^*J)\}$ where $k_1 = 2k/g_e$ and $B = 2P_d/7$.

Though g is positive for a free electron, the signs of the principal g values in the spin Hamiltonian using an effective spin for a bonded electron are not known a priori.[80] Experimentally only g_x^2, g_y^2, g_z^2, and $g_xg_yg_z$ can be determined.[80] The last quantity is invariant. For example, the negative sign of the g values of NpF_6 was determined experimentally ($g = -0.604$-(3)) by using circularly polarized radiation.[80] The convention of signs for g values of d^5 complexes with O_h symmetry is $g_x = g_y = g_z = g$.[79] Another convention is used in refs 54 and 61 (e.g., g_x, g_y, and g_z are positive for complexes with low orbital contributions—nearly pure spin g tensors).

From the hyperfine structure, the sign of $(A_xA_yA_z)$ is determined if the signs of the principal values of the D tensor (electronic quadrupole fine structure) are known; if not, only the sign of $(A_xA_yA_z)$ relative to that of $(D_xD_yD_z)$ can be found. With axial symmetry, circular polarized radiation yields the sign of $g_{||}$ uniquely, and the hyperfine structure gives the sign of $A_{||}$ relative to that of D.[80]

Application of the above-mentioned theory[79] to the published ESR data[18] results in a positive Fermi contact term (K_k) of 89 MHz for $V(CO)_6$ of D_{4h} symmetry, which would imply a strong 4s admixture into the $3d_{xy}$ orbital. Since in D_{4h} symmetry $3d_{xy}$ and 4s belong to the B_{2g} and A_{1g} irreducible representations, respectively, these orbitals cannot mix, and distortion to D_{4h} is thus ruled out. However, when D_{3d} distortion with a singly occupied $3d_{z^2}$ orbital is assumed, the parameters derived from theoretical considerations (Table 7) agree nicely with our ab initio data in Tables 2, 3, and 6. Furthermore, according to the ligand-field model,[79] the observed $g_\perp$ and $g_{||}$ values imply an orbital reduction factor $k = 0.64$ and a ratio $\Delta/\xi = 11.3$ (Table 7). The latter value, together with $\xi \approx 100$ cm^{-1},[78] affords an estimate for Δ of ca. 1100 cm^{-1} and hence an estimate for $E_{JT}(T) = \Delta/3$ of ca. 370 cm^{-1}, which is in good qualitative accord with our ab initio $E_{JT}(T)$ values of 500−1000 cm^{-1}. Similarly, from the observed $A_\perp$ and $A_{||}$ values, one arrives[79] at $K_k = -107.4$ MHz (corresponding to a ca. 2% 4s admixture) and $B = 2P_d/7 = 67.7$ MHz (corresponding to $k = 0.65$). Because of the small absolute value of $A_{||}$, its actual sign does not affect these results significantly. Note the consistency of the k values derived either from the g tensor or from the HFCCs, which lends further support for the D_{3d} structure as the observed energy minimum.

Parrish et al.[18] also report the low-temperature ESR spectra of $Nb(CO)_6$ and $M(N_2)_6$ (M = V, Nb) in CO and N_2 matrices, respectively. On the basis of the same analysis as that outlined above for $V(CO)_6$, D_{3d} and D_{4h} distortions can be attributed to $Nb(CO)_6$ and $M(N_2)_6$, respectively. The change in symmetry between both types of complexes is reflected in the different relative magnitudes of the absolute HFCC components ($|A_\perp| > |A_{||}|$ for D_{3d} and $|A_\perp| < |A_{||}|$ for D_{4h}; see Table 7), in agreement with the results of our ab initio calculations (Table 3).

7. Conclusions

We have applied an extensive array of experimental and theoretical methods to elucidate the ground-state structure of $V(CO)_6$, an archetypal Jahn−Teller system. High-level ab initio calculations, static and dynamic density functional computations, new experimental vibrational spectra, and a reinterpretation of ESR data from ref 18 all agree that at low temperatures (4−20 K) $V(CO)_6$ isolated in a Ne, Ar, or CO matrix shows a static Jahn−Teller distortion to a D_{3d} symmetric structure (see Figure 3). The combined evidence presented here serves to rule out the occurrence of a D_{4h} distortion mode, which had been suggested previously. The Jahn−Teller energy splitting is small so that with increasing temperature the distortion becomes more and more dynamic. The controversial discussion about the ground-state structure of $V(CO)_6$, which has lasted 40 years, appears to have reached a conclusion in this study.

Acknowledgment. This work was supported by the Deutsche Forschungsgemeinschaft, Fonds der Chemischen Industrie, and Schweizerischer Nationalfonds. The initial calculations were carried out at the University of Zürich using the local IBM RS/6000 workstations as well as the C4-Cluster at the ETH Zürich and the NEC SX-4 computer at CSCS Manno. We thank Dr. Frank Neese for making his ORCA program available and for helpful discussions.

Supporting Information Available: Calculated vibrational wavenumbers, intensities, and ^{13}CO isotopic shifts for $V(CO)_6$ in D_{3d} and D_{4h} symmetry, respectively, at the UBP86/AE1 and UBP86/AE2 levels of theory. Computed harmonic internal force constants for $V(CO)_6$, $[V(CO)_6]^-$, and $Cr(CO)_6$. Additional bands in the IR spectra of $V(CO)_6$. This material is available free of charge via the Internet at http://pubs.acs.org.

References and Notes

(1) Natta, G.; Ercoli, R.; Calderazzo, F.; Alberola, A.; Corradini, P.; Allegra, G. *Atti Accad. Naz. Lincei, Cl. Sci. Fis., Mat. Nat., Rend.* **1959**, *27*, 107.
(2) Ercoli, R.; Calderazzo, F.; Alberola, A. *J. Am. Chem. Soc.* **1960**, *82*, 2966.
(3) Bernier, J. C.; Kahn, O. *Chem. Phys. Lett.* **1973**, *19*, 414.
(4) Englman, R. *The Jahn−Teller Effect in Molecules and Crystals*; Wiley-Interscience: London, 1972.
(5) Bersuker, I. B. *The Jahn−Teller Effect and Vibronic Interactions in Modern Chemistry*; Plenum Press: New York, 1984.
(6) Bersuker, I. B.; Polinger, V. Z. *Vibronic Interactions in Molecules and Crystals*; Springer: Berlin, 1989.
(7) Haas, H.; Sheline, R. K. *J. Am. Chem. Soc.* **1966**, *88*, 3219.
(8) Keller, H. J.; Laubereau, P.; Nothe, D. *Z. Naturforsch., B: Chem. Sci.* **1969**, *24*, 257.
(9) Ford, T. A.; Huber, H.; Klotzbücher, W.; Moskovits, M.; Ozin, G. A. *Inorg. Chem.* **1976**, *15*, 1666.
(10) De Vore, T. C.; Franzen, H. F. *Inorg. Chem.* **1976**, *15*, 1318.
(11) Breeze, P. A.; Burdett, J. K.; Turner, J. J. *Inorg. Chem.* **1981**, *20*, 3369.
(12) Barton, T. J.; Grinter, R.; Thomson, A. J. *J. Chem. Soc., Dalton Trans.* **1978**, *608*.
(13) Holland, G. F.; Manning, M. C.; Ellis, D. E.; Trogler, W. C. *J. Am. Chem. Soc.* **1983**, *105*, 2308.
(14) Pratt, D. W.; Myers, R. J. *J. Am. Chem. Soc.* **1967**, *89*, 6470.
(15) Rubinson, K. A. *J. Am. Chem. Soc.* **1976**, *98*, 5188.
(16) Ammeter, H. J.; Zoller, L.; Bachmann, J.; Baltzer, P.; Gamp, E.; Bucher, R. E. D. *Helv. Chim. Acta* **1981**, *64*, 1063.
(17) Bratt, S. W.; Kassyk, A.; Perutz, R. N.; Symons, M. C. R. *J. Am. Chem. Soc.* **1982**, *104*, 490.

(18) Parrish, S. H.; Van Zee, R. V.; Weltner, W. J. *J. Phys. Chem. A* **1999**, *103*, 1025.
(19) Evans, S.; Green, J. C.; Orchard, A. F.; Saito, T.; Turner, D. W. *Chem. Phys. Lett.* **1969**, *4*, 361.
(20) Schmidling, D. G. *J. Mol. Struct.* **1975**, *24*, 1.
(21) Bellard, S.; Rubinson, K. A.; Sheldrick, G. M. *Acta Crystallogr., Sect. B* **1979**, *35*, 271.
(22) Rey, M.; Boudon, V.; Loete, M.; Asselin, P.; Soulard, P.; Manceron, L. *J. Chem. Phys.* **2001**, *114*, 10773.
(23) Therien, M. J.; Trogler, W. C. *J. Am. Chem. Soc.* **1988**, *110*, 4942.
(24) Lin, Z.; Hall, M. B. *Inorg. Chem.* **1992**, *31*, 2791.
(25) Spears, K. G.; Shang, H. *J. Phys. Chem. A* **2000**, *104*, 2668.
(26) Spears, K. G.; Sando, G. M. *J. Phys. Chem. A* **2001**, *105*, 5326−5333.
(27) Marin, T. W.; Homoelle, B. J.; Spears, K. G. *J. Phys. Chem. A* **2002**, *106*, 1152−1166.
(28) Pople, J. A.; Gill, P. M. W.; Handy, N. C. *Int. J. Quantum Chem.* **1995**, *56*, 303.
(29) Frisch, M. J.; Trucks, G. W.; Schlegel, H. B.; Gill, P. M. W.; Johnson, B. G.; Robb, M. A.; Cheeseman, J. R.; Keith, T.; Petersson, G. A.; Montgomery, J. A.; Raghavachari, K.; Al-Laham, M. A.; Zakrzewski, V. G.; Ortiz, J. V.; Foresman, J. B.; Cioslowski, J.; Stefanov, B. B.; Nanayakkara, A.; Challacombe, M.; Peng, C. Y.; Ayala, P. Y.; Chen, W.; Wong, M. W.; Andres, J. L.; Replogle, E. S.; Gomperts, R.; Martin, R. L.; Fox, D. J.; Binkley, J. S.; Defrees, D. J.; Baker, J.; Stewart, J. P.; Head-Gordon, M.; Gonzalez, C.; Pople, J. A. *Gaussian 94*, revision D.4; Gaussian, Inc.: Pittsburgh, PA, 1995.
(30) Frisch, M. J.; Trucks, G. W.; Schlegel, H. B.; Scuseria, G. E.; Robb, M. A.; Cheeseman, J. R.; Zakrzewski, V. G.; Montgomery, J. A., Jr.; Stratmann, R. E.; Burant, J. C.; Dapprich, S.; Millam, J. M.; Daniels, A. D.; Kudin, K. N.; Strain, M. C.; Farkas, O.; Tomasi, J.; Barone, V.; Cossi, M.; Cammi, R.; Mennucci, B.; Pomelli, C.; Adamo, C.; Clifford, S.; Ochterski, J.; Petersson, G. A.; Ayala, P. Y.; Cui, Q.; Morokuma, K.; Malick, D. K.; Rabuck, A. D.; Raghavachari, K.; Foresman, J. B.; Cioslowski, J.; Ortiz, J. V.; Stefanov, B. B.; Liu, G.; Liashenko, A.; Piskorz, P.; Komaromi, I.; Gomperts, R.; Martin, R. L.; Fox, D. J.; Keith, T.; Al-Laham, M. A.; Peng, C. Y.; Nanayakkara, A.; Gonzalez, C.; Challacombe, M.; Gill, P. M. W.; Johnson, B. G.; Chen, W.; Wong, M. W.; Andres, J. L.; Head-Gordon, M.; Replogle, E. S.; Pople, J. A. *Gaussian 98*, revision A.5; Gaussian, Inc.: Pittsburgh, PA, 1998.
(31) Becke, A. D. *Phys. Rev. A* **1988**, *38*, 3098.
(32) Perdew, J. P. *Phys. Rev. B* **1986**, *33*, 8822.
(33) Wachters, A. J. H. *J. Chem. Phys.* **1970**, *52*, 1033.
(34) Hay, P. J. *J. Chem. Phys.* **1977**, *66*, 4377.
(35) Hehre, W. J.; Ditchfield, R.; Pople, J. A. *J. Chem. Phys.* **1972**, *56*, 2257.
(36) Hariharan, P. C.; Pople, J. A. *Theor. Chim. Acta* **1973**, *28*, 213.
(37) Francl, M. M.; Pietro, W. J.; Hehre, W. J.; Binkley, J. S.; Gordon, M. S.; Defrees, D. J.; Pople, J. A. *J. Chem. Phys.* **1982**, *77*, 3654.
(38) Dunning, T. H. *J. Chem. Phys.* **1971**, *55*, 716.
(39) Dunning, T. H. *J. Chem. Phys.* **1989**, *90*, 1007.
(40) Jonas, V.; Thiel, W. *J. Chem. Phys.* **1995**, *102*, 8474.
(41) Jonas, V.; Thiel, W. *J. Chem. Phys.* **1996**, *105*, 3636.
(42) Purvis, G. D., III; Bartlett, R. J. *J. Chem. Phys.* **1982**, *76*, 1910−1918.
(43) Rittby, M.; Bartlett, R. J. *J. Chem. Phys.* **1988**, *92*, 3033−3036.
(44) Knowles, P. J.; Hampel, C.; Werner, H.-J. *J. Chem. Phys*. **1993**, *99*, 5219. Knowles, P. J.; Hampel, C.; Werner, H.-J. *J. Chem. Phys*. **2000**, *112*, 3106−3107 (erratum).
(45) *MOLPRO* 2000 is a package of ab initio programs written by H.-J. Werner and P. J. Knowles with contributions from R. D. Amos, A. Bernhardsson, A. Berning, P. Celani, D. L. Cooper, M. J. O. Deegan, A. J. Dobbyn, F. Eckert, C. Hampel, G. Hetzer, T. Korona, R. Lindh, A. W. Lloyd, S. J. McNicholas, F. R. Manby, W. Meyer, M. E. Mura, A. Nicklass, P. Palmieri, R. Pitzer, G. Rauhut, M. Schütz, H. Stoll, A. J. Stone, R. Tarroni, and T. Thorsteinsson.
(46) Watts, J. D.; Gauss, J.; Bartlett, R. J. *J. Chem. Phys.* **1993**, *98*, 8718−8733.
(47) Ahlrichs, R.; Bär, M.; Häser, M.; Horn, H.; Kölmel, M. *Chem. Phys. Lett.* **1989**, *154*, 165−169.
(48) Eichkorn, K.; Treutler, O.; Öhm, H.; Häser, M.; Ahlrichs, R. *Chem. Phys. Lett.* **1995**, *240*, 283.
(49) Eichkorn, K.; Weigend, F.; Treutler, O.; Ahlrichs, R. *Theor. Chem. Acc.* **1997**, *97*, 119−124.
(50) Treutler, O.; Ahlrichs, R. *J. Chem. Phys.* **1995**, *102*, 346−354.
(51) Sherwood, P.; deVries, A. H. *ChemShell—A Shell for Computational Chemistry*; CCLRC Daresbury Laboratory, 1999; see http://www.dl.ac.uk.
(52) Becke, A. D. *J. Chem. Phys.* **1993**, *98*, 5648−5642.
(53) Lee, C.; Yang, W.; Parr, R. G. *Phys. Rev. B* **1988**, *37*, 785−789.
(54) Neese, F. *ORCA*—An ab Initio, Density Functional, and Semiempirical Program Package, version 2.2, revision 14; Max-Planck-Institut für Strahlenchemie: Mülheim/Ruhr, Germany, 2002; for details of the implementation, see ref 61.
(55) Doyle, G.; Eriksen, K. A.; Van Engen, D. *Organometallics* **1985**, *4*, 2201.
(56) Jost, A.; Rees, B.; Yelon, W. B. *Acta Crystallogr., Sect. B* **1975**, *31*, 2649.
(57) Jonas, V.; Thiel, W. *Organometallics* **1998**, *17*, 353.
(58) Jonas, V.; Thiel, W. *J. Phys. Chem. A* **1999**, *103*, 1381.
(59) Pasquarello, A.; Petri, I.; Salmon, P. S.; Parisel, O.; Car, R.; Toth, E.; Powell, D. H.; Fischer, H. E.; Helm, L.; Merbach, A. E. *Science (Washington, D.C.)* **2001**, *291*, 856−859.
(60) Wetmore, S. D.; Boyd, R. J.; Eriksson, L. A.; Laaksonen, A. *J. Chem. Phys.* **1999**, *110*, 12059−12069.
(61) Neese, F. *J. Chem. Phys.* **2001**, *115*, 11080−11096.
(62) Kaupp, M.; Reviakine, R.; Malkina, O. L.; Arbuznikov, A.; Schimmelpfennig, B.; Malkin, V. G. *J. Comput. Chem.* **2002**, *23*, 794−803.
(63) In these cases, in particular for the D_{4h} form, the underlying perturbational treatment may be less reliable because of very small energy denominators: Neese, F., private communication.
(64) The addition of further, tight s and d polarization functions afforded only minor changes. Likewise, dynamic averaging over the low-temperature MD trajectory (RI-BP86/AE1 for a number of snapshots, cf. the procedure in ref 60) gave no significant difference from the equilibrium values.
(65) Munzarova, M.; Kaupp, M. *J. Phys. Chem. A* **1999**, *103*, 9966−9983.
(66) Argüello, G. A.; Grothe, H.; Kronberg, M.; Willner, H.; Mack, H.-G. *J. Phys. Chem. A* **1995**, *99*, 17525.
(67) Kornath, A. *J. Raman Spectrosc.* **1997**, *28*, 9.
(68) Ellis, J. E.; Faltynek, R. A.; Rochford, G. L.; Stevens, R. E. *Inorg. Chem.* **1980**, *19*, 1082.
(69) Calderazzo, F.; Pampaloni, G. *J. Organomet. Chem.* **1983**, *250*, C33−C35.
(70) Kündig, E. P.; Ozin, G. A. *J. Am. Chem. Soc.* **1974**, *96*, 3820.
(71) Schnermann, W.; Nakamoto, K. *J. Raman Spectrosc.* **1978**, *7*, 341.
(72) Holloway, J. H.; Stanger, G. *J. Chem. Soc., Dalton Trans.* **1988**, 1341.
(73) Claassen, H. H.; Selig, H. *Isr. J. Chem.* **1969**, *7*, 499.
(74) Weinstock, B.; Goodman, G. L. *Adv. Chem. Phys.* **1965**, *9*, 169−319.
(75) Weinstock, B.; Claassen, H. H.; Malm, J. G. *J. Chem. Phys.* **1960**, *32*, 181.
(76) Zhou, M.; Andrews, L. *J. Phys. Chem. A* **1999**, *103*, 5259.
(77) Miller, T. F., III; Strout, D. L.; Hall, M. B. *Organometallics* **1998**, *17*, 4164.
(78) Dunn, T. M. *Trans. Faraday Soc.* **1961**, *57*, 1441−1444.
(79) Bernhardt, E. A.; Komozin, P. N. *Russ. J. Inorg. Chem.* **1997**, *42*, 540−557. Bernhardt, E. A.; Komozin, P. N. *Zh. Neorg. Khim.* **1997**, *42*, 614.
(80) Abragam, A.; Bleaney, B. *Electron Paramagnetic Resonance of Transition Ions*; Clarendon Press: Oxford, U.K., 1970.